Available online at www.sciencedirect.com
ScienceDirect
Surface & Coatings Technology 201 (2006) 1495–1502
SURFACE & COATINGS TECHNOLOGY
www.elsevier.com/locate/surfcoat

Investigation of the chemical composition of the thermally grown oxide layer in thermal barrier systems with NiCoCrAlY bond coats

C. Mercer [a,*], S. Faulhaber [a], N. Yao [b], K. McIlwrath [c], O. Fabrichnaya [d]

[a] Department of Materials, University of California Santa Barbara, Santa Barbara, CA 93106-5050, USA
[b] Princeton Institute for the Science and Technology of Materials, Princeton University, Princeton, NJ 08544, USA
[c] Hitachi High Technologies America, Pleasanton, CA 94588-3355, USA
[d] Max-Planck-Institut für Metallforschung, Stuttgart, Germany

Received 15 September 2005; accepted in revised form 9 February 2006
Available online 6 March 2006

Abstract

The morphology and composition of the thermally grown oxide (TGO) layer in a thermal barrier system with a NiCoCrAlY bond coat are characterized by a combination of scanning and transmission electron microscopy, focused ion beam sectioning and energy-dispersive spectroscopy (EDS) element mapping. The investigation has revealed a complex TGO that exhibits numerous thickness inhomogeneities ('pegs'), and a sizable distribution of nano-scale second phase particles. These particles have been determined to be of two types: regions of entrained bond coat and oxides based on Y_2O_3 and HfO_2. The most probable phase makeup of the oxides is a cubic fluorite of approximate composition $4HfO_2$–Y_2O_3. Diffusion of Hf and Y from the bond coat or entrapment of bond coat elements during TGO growth are the most likely mechanisms for the formation of these oxide particles.

Keywords: Thermal barrier coatings; Thermally grown oxide; NiCoCrAlY; Energy-dispersive spectroscopy; Hafnia; Fluorite

1. Introduction

Thermal barrier coating (TBC) systems are widely employed in the hot sections of gas turbine engines to protect superalloy components from excessive temperatures [1–6]. Most systems consist of: (i) a low thermal conductivity oxide top coating, usually yttria-stabilized zirconia, and (ii) a bond coat (usually PtAl or NiCoCrAlY), which protects the superalloy substrate from high temperature oxidation via the formation of a thin, thermally grown oxide (TGO) layer, consisting primarily of α-alumina. The durability of the TBC is often dictated by spalling, governed by the growth of the TGO, due to induced misfit strains that cause delamination cracks [3–15].

In systems with two-phase NiCoCrAlY bond coats, the TGO embodies thickness heterogeneities or 'pegs' [12,16]. These imperfections have thickness up to five times the average (that is up to 10 μm) and often contain second phase constituents, such as yttria–alumina–garnet (YAG) [12] and spinel [16]. Porosity and cracks are also observed [16–19]. A recent study [20] has ascertained that failure occurs by the formation of a dominant delamination along the TGO/bond coat interface. The delamination traverses the pegs leaving islands of TGO embedded in the bond coat. The purpose of this investigation was to carry out a detailed assessment of the chemical composition of the second phases within the TGO. An appreciation of the TGO chemistry will be of assistance to the overall understanding of TGO evolution during thermal exposure, and its effect on subsequent failure.

2. Material and experimental procedures

The material used in this study was supplied by Pratt and Whitney, East Hartford, CT, in the form of cylindrical burner rig specimens, 5.9 mm in diameter (Fig. 1). The specimens were coated (over 64 mm of their length) with a bond coat of Ni–22Co–17Cr–12.5Al–0.25Hf–0.4Si–0.6Y (wt.%) (NiCoCrAlY), prior to the application of the 7% yttria-stabilized zirconia TBC layer via electron-beam physical vapour

* Corresponding author. Tel.: +1 805 893 5930.
E-mail address: cmercer@engineering.ucsb.edu (C. Mercer).

0257-8972/$ - see front matter © 2006 Elsevier B.V. All rights reserved.
doi:10.1016/j.surfcoat.2006.02.024

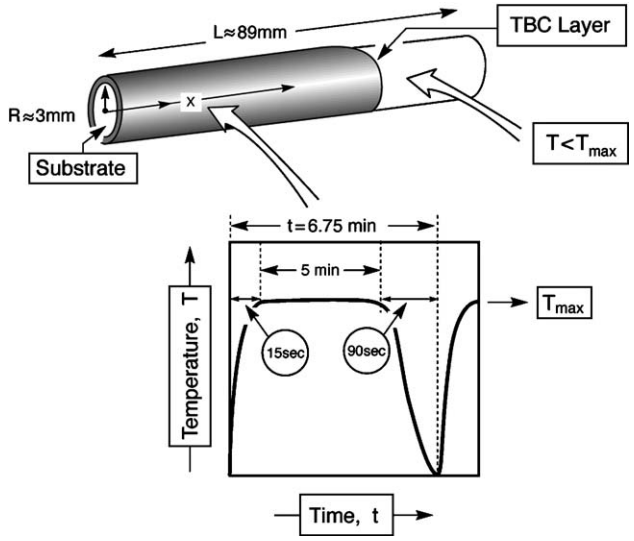

Fig. 1. Schematic illustration of burner rig specimen and heating cycle.

deposition (EB-PVD). The thickness of the TBC layer was approximately 125 μm. The substrate was PWA 1484 (Ni–5Cr–10Co–6Al–2Mo–6W–9Ta–3Re–0.5Hf (wt.%)). Following coating deposition, the specimens were subjected to thermal cycling on a burner rig apparatus, which consists of a circular carousel capable of holding 12 of the cylindrical specimens. The specimens are translated vertically one-by-one into the path of a high-velocity flame, which simulates the flame from the combustion chamber impinging on the first stage of turbine blading in an engine. Each burner cycle consists of a rapid heat up (~15 s), a 5 min exposure at peak temperature, and finally, a rapid cool (~90 s) to ambient temperature, using forced air cooling (Fig. 1).

Following mounting in Buehler Epoxicure resin, the specimens were sectioned using a Buehler precision diamond saw and metallographic prepared using SiC grinding papers prior to final diamond polishing (3 and 1 μm). Following metallographic preparation, the TGO was carefully characterized using a dual-beam FEI Strata DB 235 focused ion beam (FIB) instrument under backscattered electron imaging conditions (to provide compositional contrast). The FIB was also used to mill through selected features within the TGO to enable sub-surface examination. Finally, the FIB was employed to create transmission electron microscopy (TEM) specimens in orientations both parallel and perpendicular to the TGO, to allow detailed examination of the TGO microstructure using a Philips CM-200 TEM. The chemical composition of features within the TGO was determined using energy-dispersive spectroscopy (EDS) analysis and EDS element maps and line-scans were generated using a Hitachi HD-2300 200 kV dedicated FE-STEM system with a Thermal Noran EDS detector with a high sensitivity solid angle of 0.4 sr.

3. Observations

Cross-sectioning revealed a non-uniform TGO both morphologically and compositionally (Fig. 2). The peg thickness was typically between 5 and 10 μm, whereas the average TGO thickness is 2–3 μm. Within the pegs, porosity and various second phases are evident (Fig. 2). The TGO microstructure observed in the TEM specimen taken parallel to the TGO/TBC interface (Fig. 3), consists of very fine (up to 0.5 μm in diameter) columnar α-Al_2O_3 grains with an even distribution of second phase, nano-scale (~10–20 nm) particles within the grains. (Note, the TEM specimen was sectioned perpendicular to the long axis of the columnar grains, and so the grains appear equi-axed in Fig. 3). A TEM specimen taken through one of the larger pegs (perpendicular to the TGO/TBC interface is presented in Fig. 4. Within the peg, the microstructure was much less uniform with larger, irregularly shaped alumina grains (up to 2 μm) and a more dense distribution of the second phase particles. The particles within the peg were also observed

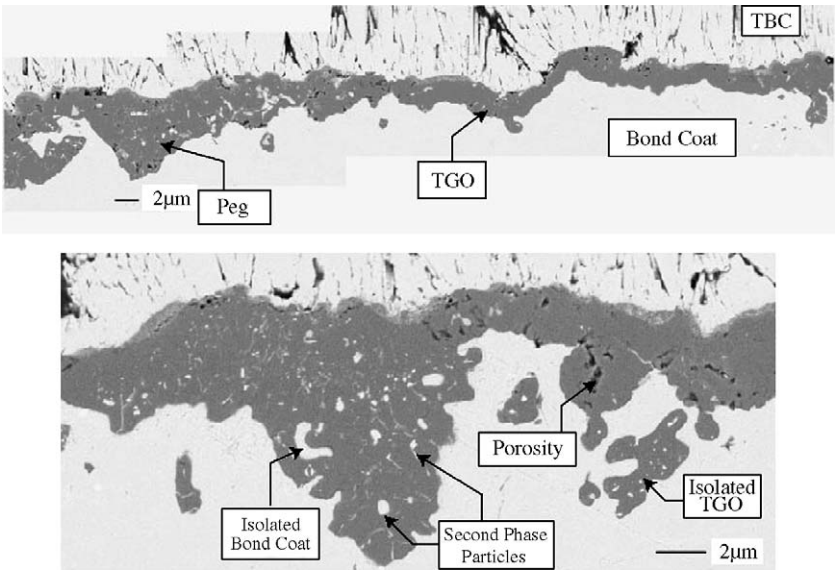

Fig. 2. TGO following burner rig testing exhibiting thickness heterogeneities or 'pegs'. Numerous second phase regions can be discerned within the pegs.

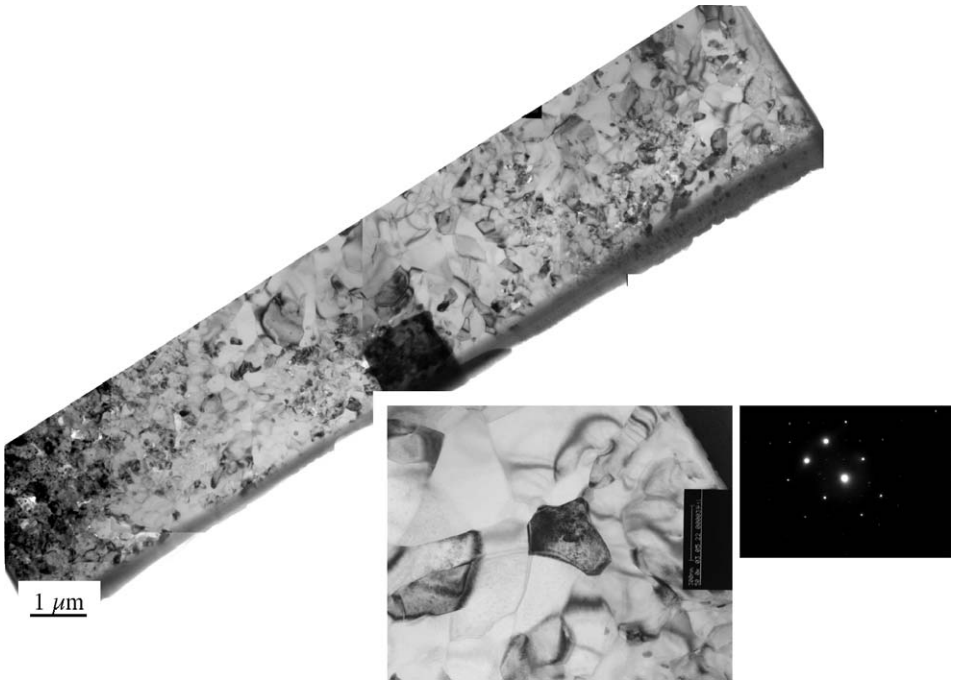

Fig. 3. TEM specimen taken through (parallel to) the regular TGO.

to have a larger size range (up to 100 nm) than those located outside the peg regions.

Energy-dispersive spectroscopy revealed the grains within the regular TGO and the peg to be composed of almost pure Al_2O_3, as expected. Two types of second phase region were discovered, however. Some of the larger (and more irregularly shaped) "particles" within the peg were determined to be regions of entrained NiCoCrAlY bond coat. Sectioning through these regions using the FIB revealed that in some cases, the bond coat regions are not really entrained but are, in fact, connected to the main bond coat. (Fig. 5). Their entrained nature is merely an artifact of the sectioning process. A typical EDS spectrum (generated in the TEM) from one of these regions is shown in Fig. 6(a). The peaks corresponding to the elements that comprise the bond coat can be clearly seen. The other second phase consisted of smaller, more spherically shaped particles. EDS analysis of these particles detected the presence of Al, Y, Hf and O (Fig. 6 (b)). The relative amounts

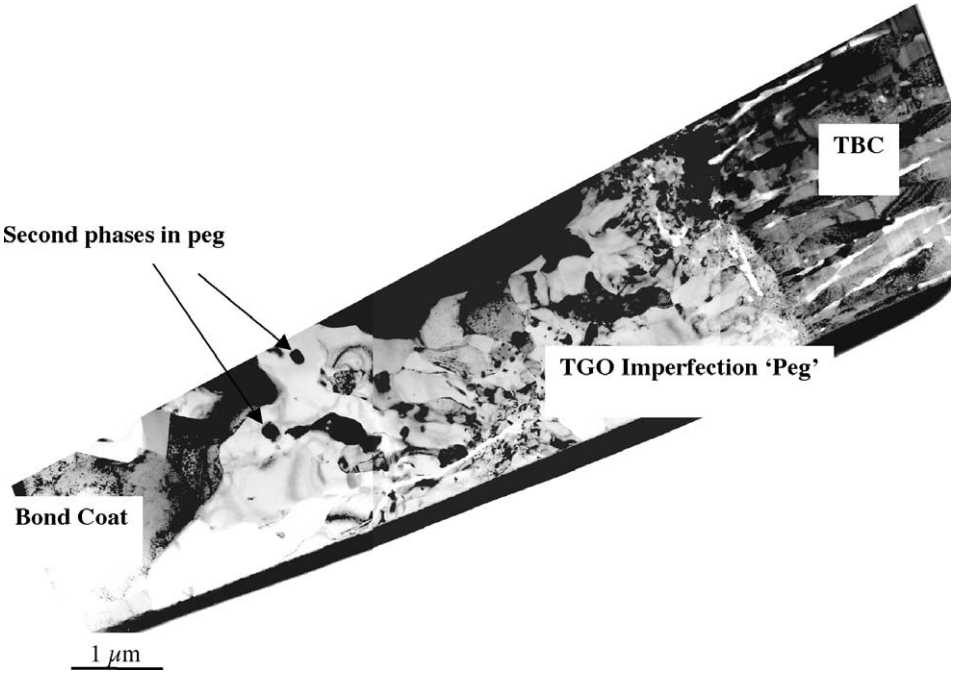

Fig. 4. TEM specimen taken through one of the larger pegs (perpendicular to TGO).

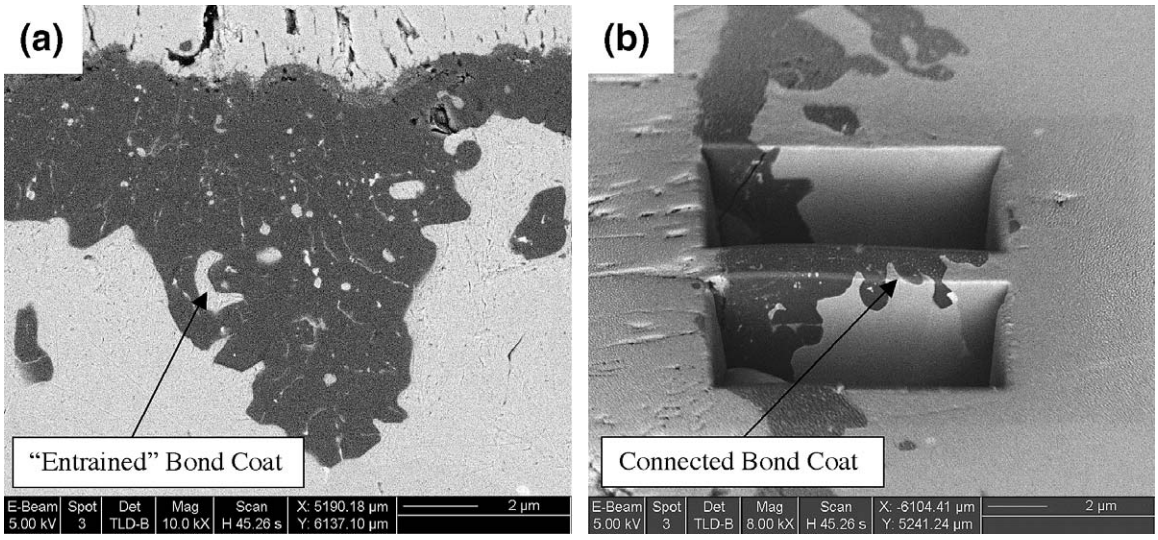

Fig. 5. (a) TGO peg showing region of "entrained" bond coat, and (b) FIB section through peg revealing that in this case, the entrained region is, in fact, connected to the main bond coat.

of these elements (determined by quantitative EDS analysis using ZAF corrections) varied somewhat between individual particles. The distribution of elements within these particles was examined using EDS element mapping within the TEM. A typical element map taken from an area within one of the pegs is shown in Fig. 7. The amounts of each element (wt.%) are also shown on the map. The Hf- and Y-rich particles can be clearly discerned. Line-scans (showing graphically the

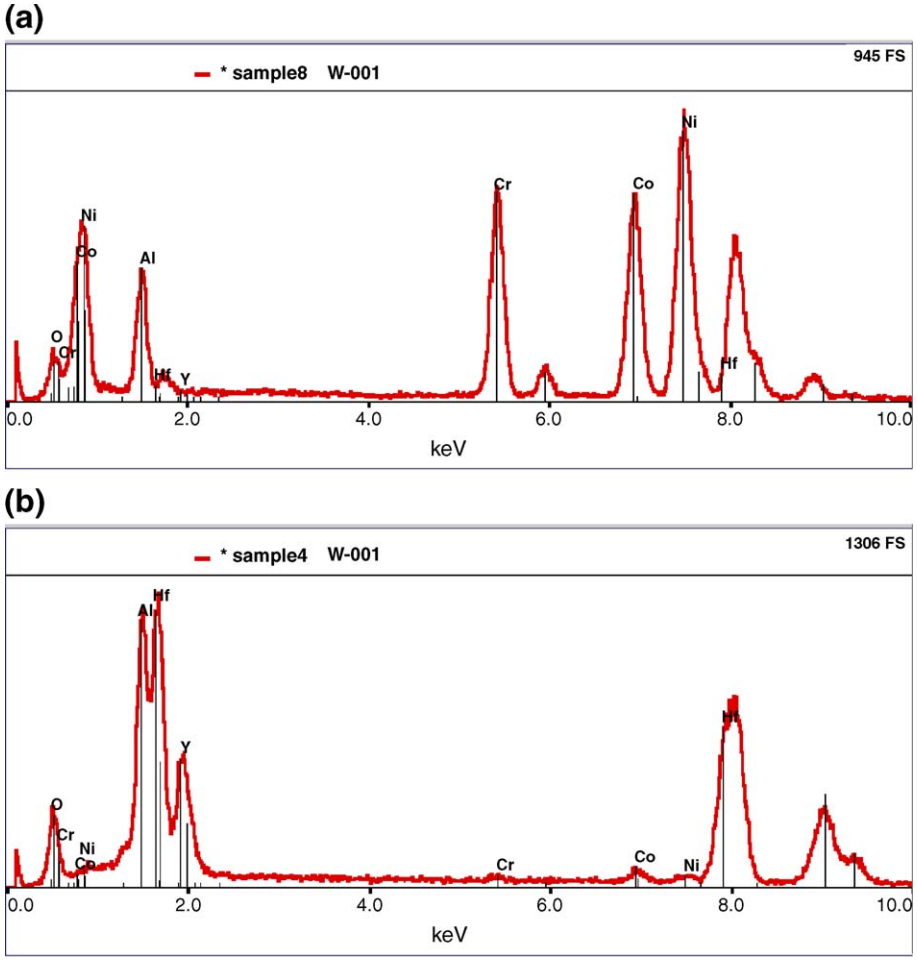

Fig. 6. EDS spectra from (a) region of entrained bond coat, and (b) Hf- , Al- and Y-rich oxide particle.

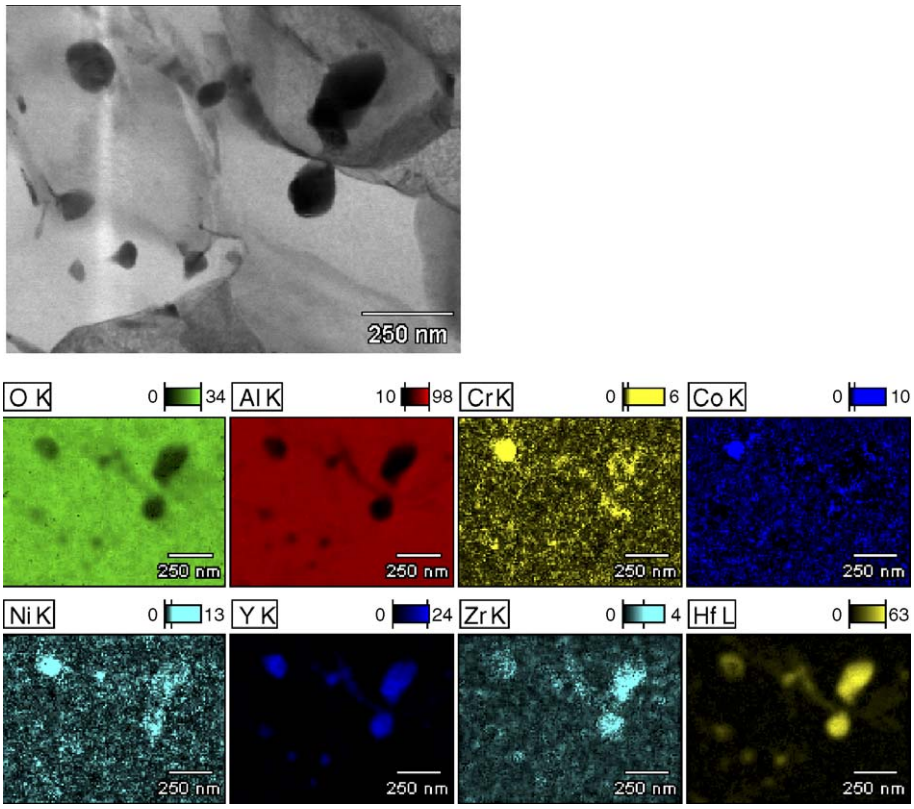

Fig. 7. EDS digital map (generated in the TEM) showing distribution of elements within the nano-scale oxide particles.

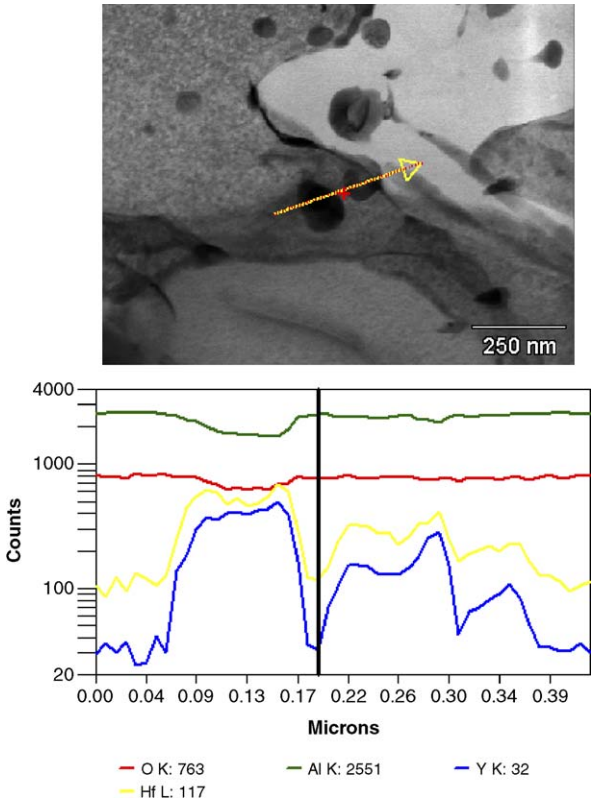

Fig. 8. Line-scan through oxide particles showing elemental (Hf, Y, Al and O) profiles.

distribution of elements along a line) were taken through selected particles (Fig. 8). The distribution of Y and Hf shows a virtually identical profile across the particles. The line-scan shown in Fig. 8 also suggests that the Al and O contents are fairly uniform both within the particles and in the surrounding TGO.

4. Phase equilibria

The TGO consists primarily of three constituents: (a) α-alumina, (b) regions of entrained NiCoCrAlY bond coat and (c) a distribution of nano-scale oxide particles rich in Al, Y and Hf. In order to determine the most likely phase composition of these particles, the yttria–hafnia–alumina ternary phase diagram (Fig. 9) was constructed from thermodynamic data obtained from the corresponding Al_2O_3–Y_2O_3, Y_2O_3–HfO_2 and HfO_2–Al_2O_3 binary phase diagrams. The details of the construction of the ternary phase diagram are reported elsewhere [21]. The composition range of the particles as determined by quantitative EDS analysis is marked by the arc on Fig. 9(a). Inspection of the ternary diagram yields two possibilities regarding the compositional nature of the various particles within the TGO: the particles consist of (i) YAG (yttria–alumina–garnet) and fluorite (a cubic HfO_2–Y_2O_3 solid solution); or (ii) the fluorite phase only (the Al detected by EDS being from the surrounding TGO). A third possibility is a metastable ternary phase, not predicted by the phase diagram. At the present time, however,

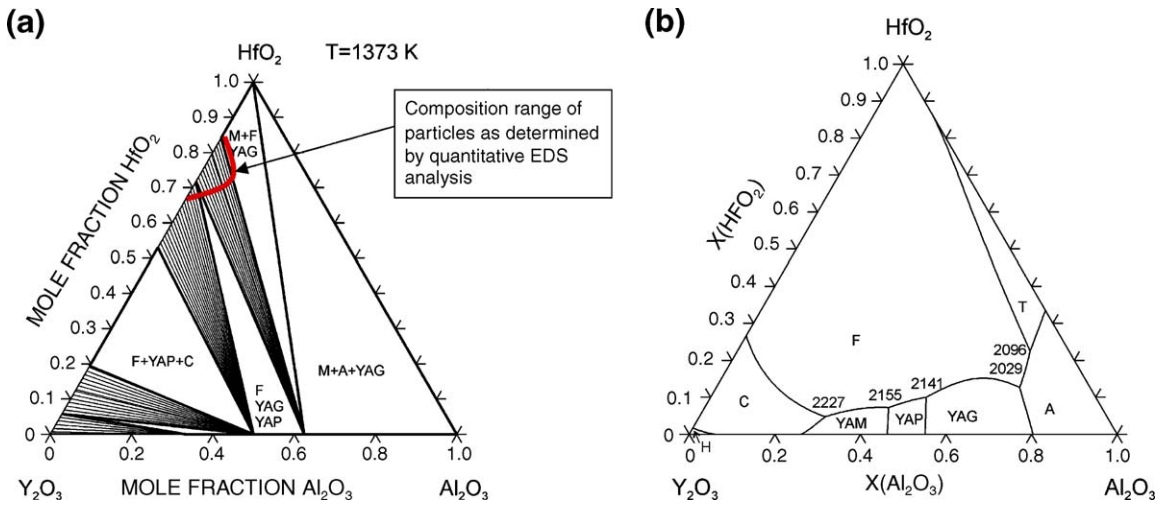

Fig. 9. The Y_2O_3–HfO_2–Al_2O_3 ternary phase diagram. (a) An isothermal section corresponding to a temperature of 1373 K, and (b) the liquidus surface.

the likelihood of the formation of a metastable ternary phase is unknown.

5. Discussion

The elements maps and line-scans give the greatest evidence as to the most likely phase makeup of the oxide particles. The distributions of Hf and Y are uniform and the profiles of these two elements across a particle have a virtually identical form. This implies that the particles are either composed of a single phase or if more than one phase is present, they are indistinguishable at the resolution of this EDS system. (The probe diameter of the Hitachi TEM used to generate the element maps and line-scans is around 2 nm). It is not completely clear whether the Al detected by EDS in actually present within the particles, or if the X-rays

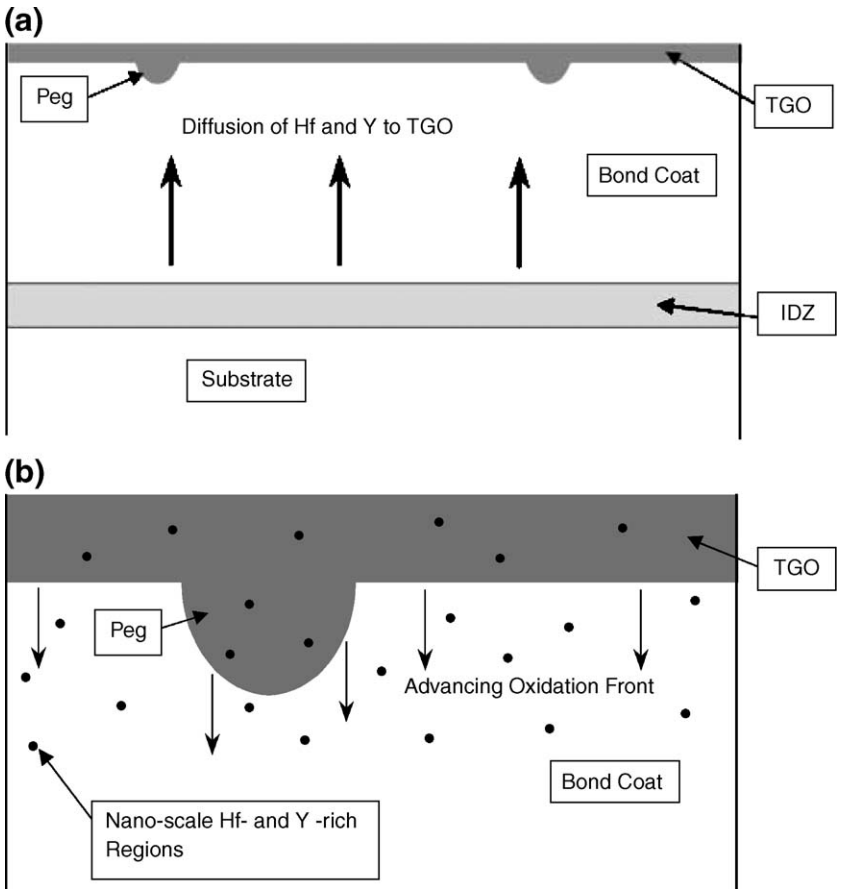

Fig. 10. Schematic illustrations showing (a) diffusion of Hf and Y into TGO from either the bond coat or substrate, and (b) entrapment of nano-scale bond coat regions rich in Hf and Y by the advancing oxidation front during TGO growth.

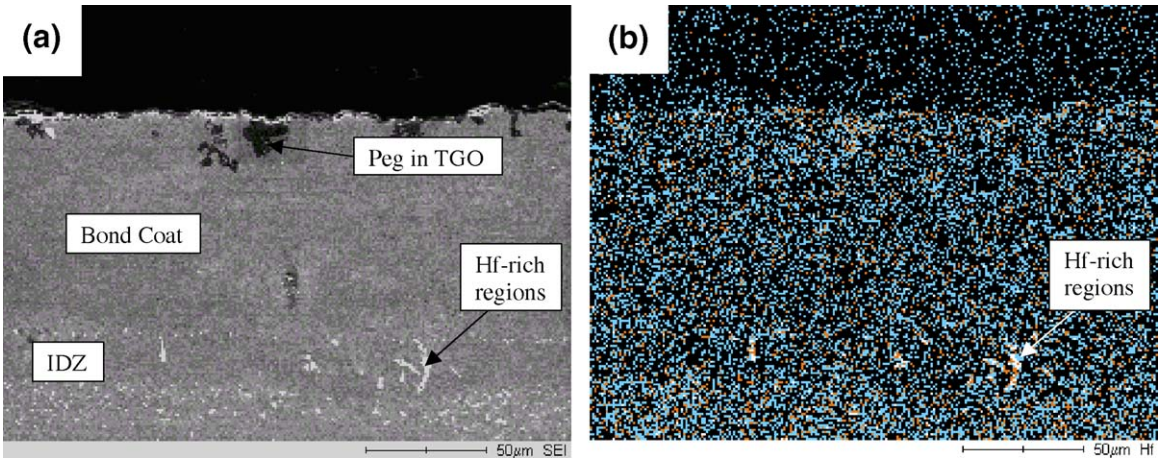

Fig. 11. (a) Secondary electron image and (b) corresponding hafnium elemental map of the bond coat and inter-diffusion zone.

corresponding to Al simply emanate from the surrounding TGO. However, since the particles are generally less than 100 nm in size, and the thickness of the TEM specimens produced by the FIB is around 100 nm, it is believed that the electron beam will pass through some of the surrounding alumina as it is traverses the specimen. Therefore, it seems most likely that the Al detected by EDS is actually from the TGO matrix and not the particles. If this is indeed the case, then the particles would be composed of only cubic HfO_2–Y_2O_3 fluorite. Eliminating the Al from the quantitative analysis, gives an approximate fluorite composition of 80% HfO_2, 20% Y_2O_3. The absence of a YAG reaction product around the HfO_2–Y_2O_3 particles might be due to non-equilibrium conditions caused by strains or interface energies.

The formation of these particles is likely due to one of two mechanisms. The first is diffusion of Hf and Y into the TGO from either the bond coat or substrate during thermal cycling (Fig. 10(a)). Subsequent precipitation, due to the very low solubility of hafnia in alumina, could then lead to the formation of the oxide particles. An EDS element map of the bond coat created using a JEOL JSM-6330F high resolution SEM (Fig. 11) has revealed the presence of Hf-rich regions in the inter-diffusion zone (IDZ) between the bond coat and the substrate. This may be the Hf source from which diffusion through the bond coat to the TGO occurs, and so the presence of a Hf-rich IDZ supports this mechanism.

The second mechanism is the entrapment of nano-scale bond coat regions rich in Hf and Y (possibly intermetallics) by the advancing oxidation front during TGO growth, followed by oxidation (Fig. 10(b)). The observation of small regions of entrained bond coat supports this mechanism, but the absence of large amounts of Ni, Co and Cr in the oxides does not. The fact that the particles within the pegs are generally intragranular also supports this entrapment idea. Diffusion followed by precipitation would normally lead to the formation of grain-boundary precipitates. But it still remains to be ascertained which of these two mechanisms is responsible for the formation of the particles.

6. Summary

The thermally grown oxide (TGO) in this TBC system was found to possess complex morphology and chemical composition following thermal cycling. Numerous thickness heterogeneities ('pegs') were observed. These pegs were up to five times the thickness of the regular TGO and contain nano-scale, second phase particles. Two types of particle have been identified: (i) regions of entrained NiCoCrAlY bond coat and (ii) oxides based on Y_2O_3 and HfO_2. Smaller Hf and Y rich oxide particles were also observed in the regular TGO. The most likely phase makeup of these oxide particles is a cubic fluorite of approximate composition $4HfO_2$–Y_2O_3. The formation of these oxide particles within the TGO is believed to be due to either to diffusion of Hf and Y from the bond coat or entrapment of nano-scale Hf- and Y-rich bond coat regions during TGO growth.

References

[1] R.A. Miller, J. Am. Ceram. Soc. 67 (1984) 517.
[2] T.E. Strangman, Thin Solid Films 127 (1985) 93.
[3] N. Padture, M. Gell, E. Jordan, Science 296 (2002) 280.
[4] M.J. Stiger, N.M. Yanar, M.G. Toppings, F.S. Pettit, G.H. Meier, Z. Met. kd. 90 (1999) 1069.
[5] P.K. Wright, Mater. Sci. Eng., A Struct. Mater.: Prop. Microstruct. Process. 245 (1998) 191.
[6] A.G. Evans, D.R. Mumm, J.W. Hutchinson, G.H. Meier, F.S. Pettit, Prog. Mater. Sci. 46 (2001) 505.
[7] J.A. Ruud, A. Bartz, M.P. Borom, C.A. Johnson, J. Am. Ceram. Soc. 84 (2001) 1545.
[8] D.R. Mumm, A.G. Evans, I.T. Spitsberg, Acta Mater. 49 (2001) 1793.
[9] I.T. Spitsberg, D.R. Mumm, A.G. Evans, Mater. Sci. Eng. A 394 (2005) 176.
[10] J.M. Ambrico, M.R. Begley, E.H. Jordan, Acta Mater. 49 (2001) 1577.
[11] A.M. Karlsson, J.W. Hutchinson, A.G. Evans, J. Mech. Phys. Solids 50 (2002) 1565.
[12] D.R. Mumm, A.G. Evans, Acta Mater 48 (2000) 1815.
[13] D.R. Mumm, M. Watanabe, A.G. Evans, J.A. Pfaendtner, Acta Mater. 52 (2004) 1123.
[14] C.A. Johnson, J.A. Ruud, R. Bruce, D. Wortman, Surf. Coat. Technol. 108/109 (1998) 80.
[15] S.R. Choi, J.W. Hutchinson, A.G. Evans, Mech. Mater. 31 (1999) 431.

[16] G.M. Kim, N.M. Yanar, E.N. Hewitt, F.S. Pettit, G.H. Meier, Scr. Mater. 46 (2002) 489.
[17] N.M. Yanar, G.H. Meier, F.S. Pettit, Scr. Mater. 46 (2002) 325.
[18] Y.H. Sohn, J.H. Kim, E.H. Jordan, M. Gell, Surf. Coat. Technol. 146/147 (2001) 70.
[19] D. Strauss, G. Muller, G. Schumacher, V. Engelko, W. Stamm, D. Clemens, W.J. Quaddakers, Surf. Coat. Technol. 135 (2001) 196.
[20] T. Xu, S. Faulhaber, C. Mercer, M. Maloney, A.G. Evans, Acta Mater. 52 (2004) 1439.
[21] O. Fabrichnaya, C. Mercer, CALPHAD 29 (2005) 239.